Rarefaction Flows and Mitigation of Imprint in Direct-Drive Implosions

I. V. Igumenshchev,[1] A. L. Velikovich,[2] V. N. Goncharov,[1] R. Betti,[1] E. M. Campbell,[1]
J. P. Knauer,[1] S. P. Regan,[1] A. J. Schmitt,[2] R. C. Shah,[1] and A. Shvydky[1]
[1]*Laboratory for Laser Energetics, University of Rochester, 250 East River Road, Rochester, New York 14623, USA*
[2]*Plasma Physics Division, Naval Research Laboratory, Washington, DC 20375, USA*

(Received 6 December 2018; revised manuscript received 7 March 2019; published 6 August 2019)

Using highly resolved 3D radiation-hydrodynamic simulations, we identify a novel mechanism by which the deleterious impact of laser imprinting is mitigated in direct-drive inertial confinement fusion. Unsupported shocks and associated rarefaction flows, commonly produced with short laser bursts, are found to reduce imprint modulations prior to target acceleration. Optimization through the choice of laser pulse with picket(s) and target dimensions may improve the stability of lower-adiabat designs, thus providing the necessary margin for ignition-relevant implosions.

DOI: 10.1103/PhysRevLett.123.065001

The 30-kJ OMEGA laser [1] is used to study implosion physics and demonstrate the achievement of ignition-equivalent conditions in energy scaled-down, direct-drive inertial confinement fusion (ICF) experiments [2]. These experiments indicate that implosions of spherical-shell targets can suffer from mass modulations imposed by nonuniformities in the laser. These modulations can be divided into groups of low (with Legendre modes $\ell \lesssim 30$) and high ($\ell \gtrsim 30$) modes based on mechanisms of amplification used during the target acceleration phase [3]. High-mode modulations can quickly grow because of the Rayleigh-Taylor (RT) instability [4], whereas low-mode modulations (which have sufficiently large spatial scales and remain hydrodynamically decoupled) undergo the relatively slow secular and Bell-Plesset [5] growths.

High-mode modulations are "imprinted" by laser speckles. The imprint spectrum is formed during the imprint phase ("Phase 1"), beginning with the laser pulse and ending with a shock break out at the inner edge of an imploding shell. In the following target acceleration "Phase 2", the spectrum evolves almost self-similarly (see below) because of the ablative RT growth of the modulation amplitude A_ℓ^0 developing during Phase 1, $A_\ell(t) = A_\ell^0 \exp(\int \gamma_\ell dt)$, where γ_ℓ is the growth rate [6,7]. Apparently, imprint can be mitigated by reducing A_ℓ^0 in Phase 1 and/or γ_ℓ in Phase 2.

High-performance implosions require shaped laser pulses, like ramp pulses [8], resulting in low-adiabat (adiabat $\alpha = P/P_F \lesssim 3$, the ratio of the pressure to the Fermi-degenerated gas pressure [3]) and high in-flight aspect ratio (IFAR $\gtrsim 25$, the ratio of the shell radius at $2/3$ of the initial radius to the shell thickness [9]) imploding shells. Such shells, however, were found to be notoriously unstable, leading to degraded performance, and several techniques were proposed to fix this. It was suggested [10] and experimentally verified [11,12] that a low-intensity laser prepulse can improve stability. Other proposed smoothing techniques employ targets with a low-density foam overcoat [13] and with corona preformed by external x rays [14] or formed by layers with high-Z dopant [15]. Improved stability was predicted for stratified shells [16–19]. Present-day experiments use picket pulses, which achieve higher performance [20,21]. This advantage was attributed to a spatially-varying adiabat ("adiabat shaping") that reduces γ_ℓ in Phase 2 [21–24]. However, our work identifies an entirely distinct additional (and often dominant) aspect of the overall mechanism by which the burst structure of the drive reduces A_ℓ^0 prior to Phase 2.

In this Letter, a novel mechanism playing a dominant role in imprint mitigation in ICF implosions driven by picket pulses is described. This mechanism involves unsupported shocks, which are produced by these pulses, and rarefaction flows after these shocks. Rarefaction flows play a key role in mitigating imprint because of their known properties to suppress areal mass modulations [25,26]. This mechanism can efficiently suppress the entire range of dangerous imprint modes $\ell \gtrsim 30$ in Phase 1, consequently providing low seeds for the RT growth in Phase 2. Adiabat shaping plays only a secondary role by helping to reduce the growth of modes $\ell \gtrsim 100$ (see Fig. 4 in Ref. [21]). Understanding the new mechanism can lead to better strategies for providing the necessary margin in direct- and indirect-drive [27,28] ICF.

Rarefaction flows are known to be neutrally stable at the leading edge and unstable at the trailing (low-density) edge, oscillating with the local sound frequency and amplitude growing in time [25,26]. Areal mass in rarefaction flows experiences decaying oscillations, indicating that perturbations in density and pressure are localized at the trailing edge [29–32]. Figure 1 illustrates the development of imprint modulations in imploding shells compressed by supported and unsupported shocks, which are produced by continuous and picket pulses, respectively. The green area at the ablation front indicates the location of modulations

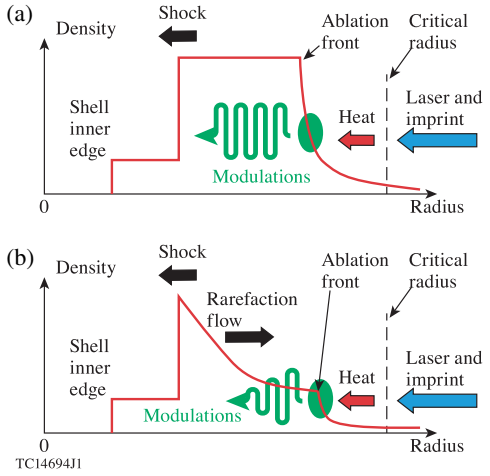

FIG. 1. (a) Imprint modulations (the green area) localized at the ablation front can feed-through to an imploding shell compressed by a supported shock, and (b) cannot do this in a shell compressed by a unsupported shock.

originating from laser nonuniformities. These modulations can feed-through to the shell (to the left) in the case of a supported shock [Fig. 1(a)] and cannot do this in the case of a unsupported shock, which develops a post-shock rarefaction flow [Fig. 1(b)]. As a result, imprint is only mitigated in the latter case, in which modulations are localized near the ablation front and moved away (to the right) with the ablating mass.

To demonstrate the new mechanism, consider 3D radiation-hydrodynamic simulations using the code ASTER [33] of two implosion designs, which assume different laser pulses, but are characterized by similar moderately low adiabat (≈3) and moderately high IFAR (≈28) and demonstrate similar 1D performance. These designs assume identical targets consisting of a spherical deuterium-tritium (DT) ice layer and a plastic [carbon-deuterium (CD)] overcoat [see Fig. 2(a)] and use pulses with a short picket or continuous foot before the main pulse [see Fig. 2(b) in blue and red]. The higher intensity of the picket compared to the foot results in adiabat shaping [21], which reduces the RT growth of higher modes $\ell \gtrsim 100$ but does not affect the seeding [34] and growth of lower modes we are interested in, see below. Simulations show that imprint is not mitigated in the no-picket design, resulting in its poor performance and substantially mitigated in the single-picket one. Note that simulations using these laser pulses and uniform-shell targets (all DT) indicate that the described mechanism is independent of the presence of material interfaces.

ASTER is an Eulerian hydrodynamic code implementing on the spherical moving grid. It models the dynamics of two-temperature (for ions and electrons), multispecious plasma and includes flux-limited multigroup diffusion radiation transfer, flux-limited diffusion heat transport for ions and electrons, simplified laser ray-tracing with

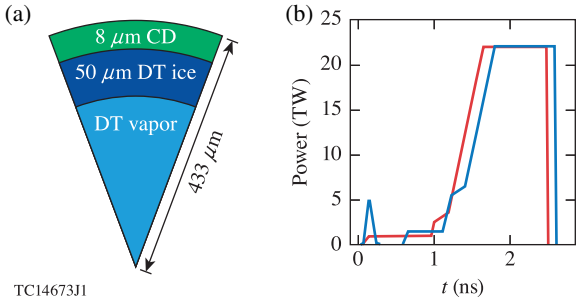

FIG. 2. (a) The target and (b) the single-picket (in blue) and no-picket (in red) laser pulses of 26 kJ each for OMEGA cryogenic implosion designs.

cross-beam energy transfer [35] and inverse bremsstrahlung, selected nuclear reactivity, and tabulated material properties. ASTER is characterized by a low numerical noise suitable for studying linear and nonlinear broad-band modulations. Simulations assume the OMEGA 60-beam illumination pattern, which introduces distinctive low-mode $\ell = 10$ and 18 features in modulation spectra, and use the speckle-based model of imprint [36]. They also apply three OMEGA laser-smoothing techniques: distributed phase plates [37,38], polarization smoothing [39], and smoothing by spectral dispersion [40]. In simulations, modes ℓ up to ≃200 are well resolved, while the resolution of higher modes can suffer, resulting in underestimation of the amplitude (by a factor of ∼2 at $\ell = 400$).

First, consider the no-picket design, in which the shell is compressed by supported shocks and imprint is not mitigated in both Phases 1 [as illustrated in Fig. 1(a)] and 2 (no adiabat shaping). Figure 3 shows the evolution of the spectrum of areal mass modulations (normalized to the shell average density and given in the units of microns) in this design at $t = 0.2$, 0.5, and 1.4 ns. Mass modulations at $t = 0.2$ ns are directly induced by nonuniformities in the laser and have a dominant high-mode component. At a later time, when mass modulations evolve independently from laser nonuniformities (these two decouple after $t \simeq 100$ ps), the spectrum evolves such that modes in the range of $\ell \sim 100$ to 200 grow most efficiently and become dominant [see Figs. 3(b) and 3(c)]. This growth is in good agreement with predictions of the imprint model in Ref. [41], in which modulations at the ablation front feed-through to a shock-compressed shell of uniform density and pressure. The late-time reduction of the high-mode ($\ell \gtrsim 200$) spectrum tail [Fig. 3(c)] can be explained by a phase inversion caused by the ablative Richtmyer-Meshkov instability (RMI) [42–44]. This inversion is relatively slow because of the assumed laser intensity profile and apparently inefficient for suppressing the growth of modes $\ell \lesssim 200$.

The spectrum in Fig. 3(c) plotted for the end of Phase 1, the time of shock breakout at 1.4 ns, represents the initial imprint amplitudes A_ℓ^0 amplified during Phase 2. In this phase, the spectrum evolves in a "self-similar" manner, in which it is not significantly changed in the shape but

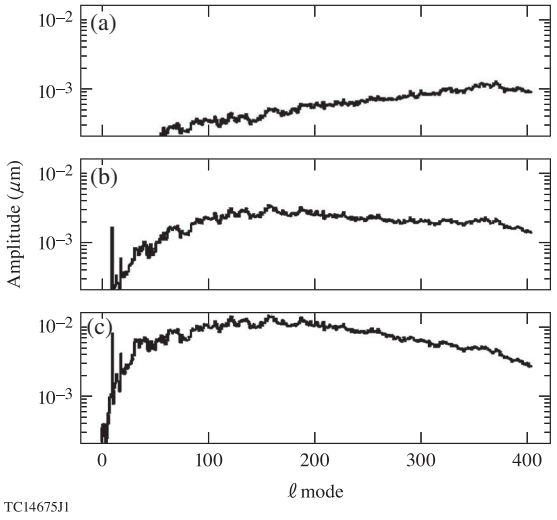

FIG. 3. Spectrum of areal mass modulations from 3D simulations of the design using the no-picket pulse shown in red in Fig. 2(b): (a) $t = 0.2$ ns, (b) 0.5 ns, and (c) 1.4 ns.

increases its magnitude. This is the result of the ablative RT growth, in which the growth of high modes $\ell \gtrsim 100$ is reduced [45]. The self-similar evolution ends when the dominant modes experience the nonlinear RT growth.

The single-picket pulse compresses the shell by an unsupported shock, which develops post-shock rarefaction flow, as illustrated in Fig. 1(b), and shows apparently different evolution of the spectrum (Fig. 4). While the spectra in Figs. 3(a) and 4(a) looks similar, the later-time evolution of the spectrum in Fig. 4 is characterized by relatively fast phase inversions of imprint modes. These inversions can be observed as a dip in the spectrum, propagating with time from high to low modes. This dip locates at $\ell \simeq 300$ in $t = 0.4$ ns, $\ell \simeq 150$ in $t = 0.6$ ns, and $\ell \simeq 80$ in $t = 1.0$ ns [see Figs. 4(b)–4(d), respectively]. The inversion dip corresponds to sonic oscillations of areal mass, when the amplitude of a given mode goes through the zero-point. The faster oscillations of higher modes cause this dip to propagate in time from high to low modes. The important consequence of the inversions is that involved modes are reduced in the amplitude. These inversions and amplitude reduction are indicators of decaying areal mass oscillations in rarefaction flows discussed earlier. The ablative RMI likely affects modes $\ell \gtrsim 200$ by reducing them, as it does in the no-picket design. It is difficult, however, to distinguish this effect from the effect of rarefaction flows.

The spectrum in Fig. 4(e), like in Fig. 3(c), is plotted for the time of shock breakout (1.45 ns in this case), but it is substantially different from that in Fig. 3(c). The amplitudes A_ℓ^0 represented by this spectrum take the maximum at $\ell \simeq 30$ and decrease toward higher ℓ modes. These maximum modes continue to dominate in Phase 2 and reach the nonlinear stage earlier than other high modes. This is because the reduction in A_ℓ^0 overcomes the RT growth $\propto \exp(\int \gamma_\ell dt)$ at $\ell \gtrsim 30$.

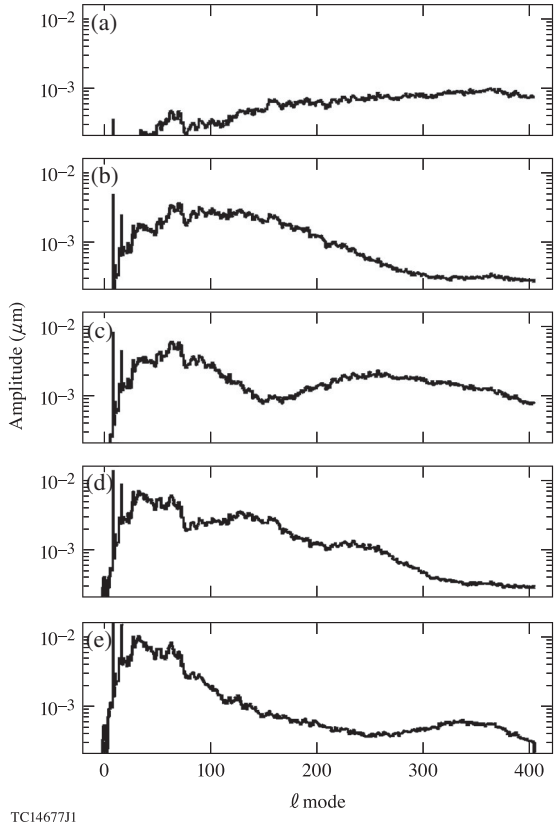

FIG. 4. Same as in Fig. 3, but using the single-picket pulse shown in blue in Fig. 2(b): (a) $t = 0.2$ ns, (b) 0.4 ns, (c) 0.6 ns, (d) 1.0 ns, and (e) 1.45 ns.

Figures 5(a) and 5(b) show density cross-sections from simulations of the no-picket and single-picket designs in the end of Phase 2 and prior to the deceleration phase (at $t = 2.45$ and 2.55 ns, respectively). The large-amplitude RT density spikes and bubbles in Fig. 5(a) correspond to dominant modes $\ell \sim 100$ to 200, which were developed to the end of Phase 1 [Fig. 3(c)]. These spikes and bubbles produce a "broken shell", in which the thickness increases by a factor of ~5 with respect to the 1D counterpart. The broken shell has an increased "effective" adiabat and, as a result, the shell stagnates at the radius by a factor of 2 larger ($\simeq 40$ μm vs $\simeq 20$ μm in 1D). Such an undercompression results in a substantial loss in performance: neutron yield $Y_n = 2.37 \times 10^{13}$ (13% of the 1D value) and neutron-averaged areal mass $\langle \rho R \rangle_n = 92$ mg/cm^2 (37%). Contrary to that, the shell in Fig. 5(b) has strongly reduced high-mode modulations. This reduction is entirely due to the perturbation-seeding Phase 1. It translates into mitigating the effects of imprint on the implosion: $Y_n = 8.40 \times 10^{13}$ (46% of the 1D value) and $\langle \rho R \rangle_n = 207$ mg/cm^2 (81%).

Implosion designs are optimized in 1D by matching the laser pulse strength and timing and target dimensions. Optimum picket designs showing the best 1D performance use low-energy first pickets corresponding to very low-α implosions ($\alpha \lesssim 2$). Such pickets, however, produce

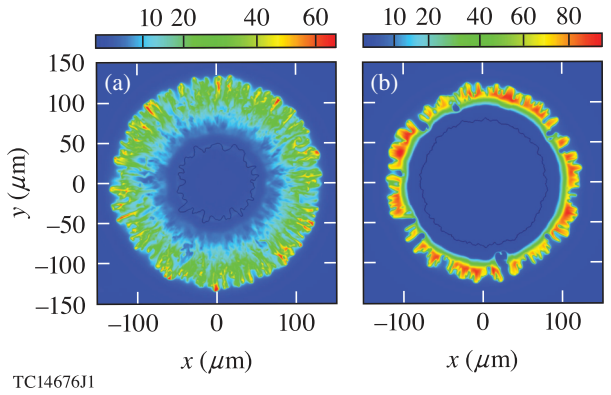

FIG. 5. Meridional cross sections of the distribution of density (in g/cm^3) from 3D simulations of the designs using the (a) no-picket and (b) single-picket pulses shown in Fig. 2(b) in red and blue, respectively. The images are shown at $t = 2.45$ and 2.55 ns, respectively, corresponding to moments prior to deceleration of the targets.

relatively weak leading shocks, followed by also weak rarefaction flows (with reduced release velocities), which can not sufficiently mitigate imprint because of a lack of suppression of the inward modulation feed-through. Imprint is mitigated by stronger pickets, which produce more powerful rarefaction flows, but, in turn, increase adiabat and consequently reduce 1D performance. On the other hand, too strong pickets cannot efficiently mitigate imprint because of shortening the time separating the first picket and main pulse, so that the spectrum inversion dip has no time to propagate all the way down to $\ell \sim 30$. Therefore, optimum 3D implosions require medium-strength first pickets. The optimum picket strength was found in experiments and, for the current OMEGA setup, corresponds to $\alpha \sim 3$ designs. It is worth noting that a rarefaction flow produced by the first picket has a major effect on the imprint, which is much less affected by other pickets in multipicket implosion designs. This conclusion is in a good agreement with OMEGA experiments showing similar performances of optimized $\alpha \sim 3$ implosions using either single- or triple-picket pulses of the same total energy.

To illustrate the importance of first picket strength, consider simulations of two OMEGA shots 69236 and 77066 ($\alpha \approx 2$ and 3, respectively), which use triple-picket pulses, as shown in Fig. 6(a) and targets in Fig. 2(a). Figure 6(b) compares modulation spectra in the end of Phase 1. Shot 69236 has the small-energy first picket developing a weak rarefaction flow. As a result, imprint modes experience phase inversion [note the dip at $\ell \approx 80$ in the spectrum in red in Fig. 6(b)], but modes $\ell \simeq 150$ continue to grow and become dominant. The shell in the end of Phase 2 is broken and similar to that in Fig. 5(a). This implosion suffers from imprint: $Y_n = 1.23 \times 10^{13}$ (6.5% of the 1D value), which agrees well with the measured $Y_n = (1.08 \pm 0.05) \times 10^{13}$. Note the apparent failure of adiabat shaping in this implosion. Shot 77066 has

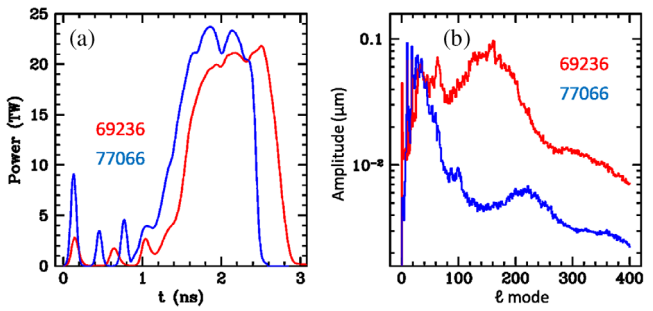

FIG. 6. (a) Laser pulses and (b) simulated spectra of areal mass modulations for OMEGA shots 69236 (in red) and 77066 (in blue), respectively. These spectra are taken at $t = 2.04$ and 1.81 ns corresponding to shells' initial acceleration.

the higher-energy first picket and optimum timing of the inversion dip, causing reduction of imprint modes down to $\ell \simeq 30$ [see Fig. 6(b) in blue]. This minimizes the effects of imprint, resulting in $Y_n = 9.78 \times 10^{13}$ (72% of the 1D value). This simulated yield, however, is by a factor of 2.4 larger than the measured one [46], indicating that other reduction mechanisms are in effect.

In summary, 3D ASTER simulations help to identify a novel mechanism that is responsible for mitigating imprint modes $\ell \gtrsim 30$ in direct-drive implosions with picket laser pulses. This mechanism involves rarefaction flows developing by unsupported shocks. Rarefaction flows can result in a decay of imprint modulations during the imprint phase, consequently reducing seeds for the RT growth at the following acceleration phase. Adiabat shaping plays a secondary role, reducing the RT growth of modes $\ell \gtrsim 100$. Optimization through the choice of pulse shape and target dimensions may improve the efficiency of the new mechanism. Simulations suggest that beside imprint other effects, such as low-mode nonuniformities coming from laser and target asymmetries, perturbations from stalk mount and surface defects, and uncertainties in 1D physics, can still remain a major drawback to the achievement of ignition-relevant conditions in direct-drive ICF [47].

This material is based upon work supported by the Department of Energy National Nuclear Security Administration under Award No. DE-NA0003856, the University of Rochester, and the New York State Energy Research and Development Authority.

This report was prepared as an account of work sponsored by an agency of the U.S. Government. Neither the U.S. Government nor any agency thereof, nor any of their employees, makes any warranty, express or implied, or assumes any legal liability or responsibility for the accuracy, completeness, or usefulness of any information, apparatus, product, or process disclosed, or represents that its use would not infringe privately owned rights. Reference herein to any specific commercial product, process, or service by trade name, trademark, manufacturer, or otherwise does not necessarily constitute or imply its endorsement,

[1] T. R. Boehly, D. L. Brown, R. S. Craxton *et al.*, Opt. Commun. **133**, 495 (1997).
[2] V. N. Goncharov, S. P. Regan, E. M. Campbell *et al.*, Plasma Phys. Controlled Fusion **59**, 014008 (2017).
[3] S. Atzeni and J. Meyer-ter-Vehn, *The Physics of Inertial Fusion: Beam Plasma Interaction, Hydrodynamics, Hot Dense Matter*, International Series of Monographs on Physics (Clarendon, Oxford, 2004), pp. 52,56,278.
[4] L. Rayleigh, Proc. London Math Soc. **s1**–**s14**, 170 (1883); G. Taylor, Proc. R. Soc. Ser. A **201**, 192 (1950).
[5] G. I. Bell, Los Alamos National Laboratory, Los Alamos, Report LA-1321 (1951) (unpublished); M. S. Plesset, J. Appl. Phys. **25**, 96 (1954).
[6] S. Bodner, Phys. Rev. Lett. **33**, 761 (1974).
[7] H. Takabe, K. Mima, L. Montierth, and R. L. Morse, Phys. Fluids **28**, 3676 (1985).
[8] S. E. Bodner, D. G. Colombant *et al.*, Phys. Plasmas **5**, 1901 (1998).
[9] V. N. Goncharov, T. C. Sangster, R. Betti *et al.*, Phys. Plasmas **21**, 056315 (2014).
[10] W. C. Mead and J. D. Lindl, Bull. Am. Phys. Soc. **21**, 1102 (1976).
[11] A. B. Iskakov, V. F. Tishkin, I. G. Lebo, J. Limpouch, K. Mašek, and K. Rohlena, Phys. Rev. E **61**, 842 (2000).
[12] E. Krouský, O. Renner, K. Mešek, M. Pfeiffer, O. Pacherová, B Kraliková, J. Skála, and K. Rohlena, Laser Part. Beams **18**, 87 (2000).
[13] M. Desselberger, M. W. Jones, J. Edwards, M. Dunne, and O. Willi, Phys. Rev. Lett. **74**, 2961 (1995).
[14] M. Nishikino, H. Shiraga, N. Miyanaga *et al.*, Phys. Plasmas **9**, 1381 (2002).
[15] S. X. Hu, G. Fiksel, V. N. Goncharov, S. Skupsky, D. D. Meyerhofer, and V. A. Smalyuk, Phys. Rev. Lett. **108**, 195003 (2012).
[16] K. O. Mikaelian, Phys. Rev. A **28**, 1637 (1983).
[17] K. O. Mikaelian, Phys. Rev. A **42**, 3400 (1990).
[18] N. Metzler, A. L. Velikovich, and J. H. Gardner, Phys. Plasmas **6**, 3283 (1999).
[19] N. Metzler, A. L. Velikovich, A. J. Schmitt, and J. H. Gardner, Phys. Plasmas **9**, 5050 (2002).
[20] T. J. B. Collins and S. Skupsky, Phys. Plasmas **9**, 275 (2002).
[21] V. N. Goncharov, J. P. Knauer, P. W. McKenty, P. B. Radha, T. C. Sangster, S. Skupsky, R. Betti, R. L. McCrory, and D. D. Meyerhofer, Phys. Plasmas **10**, 1906 (2003).
[22] N. Metzler, A. L. Velikovich, A. J. Schmitt, M. Karasik, V. Serlin, A. N. Mostovych, S. P. Obenschain, J. H. Gardner, and Y. Aglitskiy, Phys. Plasmas **10**, 1897 (2003).
[23] K. Anderson and R. Betti, Phys. Plasmas **11**, 5 (2004).
[24] T. J. B. Collins, J. P. Knauer, R. Betti, T. R. Boehly, J. A. Delettrez, V. N. Goncharov, D. D. Meyerhofer, P. W. McKenty, S. Skupsky, and R. P. J. Town, Phys. Plasmas **11**, 1569 (2004).
[25] Y. Yang, Q. Zhang, and D. Sharp, Phys. Fluids **6**, 1856 (1994).
[26] A. Velikovich and L. Phillips, Phys. Fluids **8**, 1107 (1996).
[27] J. L. Peterson, D. S. Clark, L. P. Masse, and L. J. Suter, Phys. Plasmas **21**, 092710 (2014).
[28] V. A. Smalyuk, H. F. Robey, T. Döppner *et al.*, Phys. Plasmas **23**, 102703 (2016).
[29] A. L. Velikovich, A. J. Schmitt, J. H. Gardner, and N. Metzler, Phys. Plasmas **8**, 592 (2001).
[30] A. L. Velikovich, A. J. Schmitt, N. Metzler, and J. H. Gardner, Phys. Plasmas **10**, 3270 (2003).
[31] A. L. Velikovich, S. T. Zalesak, N. Metzler, and J. G. Wouchuk, Phys. Rev. E **72**, 046306 (2005).
[32] Y. Aglitskiy, M. Karasik, A. L. Velikovich, V. Serlin, J. Weaver, T. J. Kessler, A. J. Schmitt, S. P. Obenschain, N. Metzler, and J. Oh, Phys. Rev. Lett. **109**, 085001 (2012).
[33] I. V. Igumenshchev, V. N. Goncharov, F. J. Marshall *et al.*, Phys. Plasmas **23**, 052702 (2016).
[34] R. Ishizaki and K. Nishihara, Phys. Rev. Lett. **78**, 1920 (1997).
[35] I. V. Igumenshchev, D. H. Edgell, V. N. Goncharov, J. A. Delettrez, A. V. Maximov, J. F. Myatt, W. Seka, A. Shvydky, S. Skupsky, and C. Stoeckl, Phys. Plasmas **17**, 122708 (2010).
[36] R. Epstein, J. Appl. Phys. **82**, 2123 (1997).
[37] Y. Kato, K. Mima, N. Miyanaga, S. Arinaga, Y. Kitagawa, M. Nakatsuka, and C. Yamanaka, Phys. Rev. Lett. **53**, 1057 (1984).
[38] T. J. Kessler, Y. Lin, J. J. Armstrong, and B. Velazquez, Proc. SPIE Int. Soc. Opt. Eng. **1870**, 95 (1993).
[39] T. R. Boehly, V. A. Smalyuk, D. D. Meyerhofer, J. P. Knauer, D. K. Bradley, R. S. Craxton, M. J. Guardalben, S. Skupsky, and T. J. Kessler, J. Appl. Phys. **85**, 3444 (1999).
[40] S. Skupsky and R. S. Craxton, Phys. Plasmas **6**, 2157 (1999).
[41] R. Ishizaki and K. Nishihara, Phys. Rev. E **58**, 3744 (1998).
[42] V. N. Goncharov, Phys. Rev. Lett. **82**, 2091 (1999).
[43] V. N. Goncharov, S. Skupsky, T. R. Boehly, J. P. Knauer, P. McKenty, V. A. Smalyuk, R. P. J. Town, O. V. Gotchev, R. Betti, and D. D. Meyerhofer, Phys. Plasmas **7**, 2062 (2000).
[44] V. N. Goncharov, O. V. Gotchev, E. Vianello *et al.*, Phys. Plasmas **13**, 012702 (2006).
[45] R. Betti, V. N. Goncharov, R. L. McCrory, and C. P. Verdon, Phys. Plasmas **5**, 1446 (1998).
[46] S. P. Regan, V. N. Goncharov, I. V. Igumenshchev *et al.*, Phys. Rev. Lett. **117**, 025001 (2016).
[47] I. V. Igumenshchev, D. T. Michel, R. C. Shah *et al.*, Phys. Plasmas **24**, 056307 (2017).